

## THE ROLE OF DEPOSITION TEMPERATURE ON PARTICLE SIZE, ROUGHNESS PARAMETERS, MAGNETIC AND STRUCTURAL FEATURES OF ELECTROCHEMICALLY GROWN Ni-Fe/ITO SAMPLES

U. SARAÇ<sup>a,\*</sup>, M. KAYA<sup>b</sup>, M. C. BAYKUL<sup>c</sup>

<sup>a</sup>Department of Science Education, Bartın University, 74100, Bartın, Turkey

<sup>b</sup>Vocational School of Health Service, Eskişehir Osmangazi University, 26480, Eskişehir, Turkey

<sup>c</sup>Department of Metallurgical and Materials Engineering, Eskişehir Osmangazi University, 26480, Eskişehir, Turkey

In this work, the impact of the deposition temperature (DT) on the particle size, roughness parameters, coercive force, squareness and structural features of the Ni-Fe samples electrochemically deposited onto glasses covered with indium tin oxide (ITO) was researched. An increase in the DT from 20 to 40 °C led to a very slight increase in the Fe concentration of the samples, revealing that the effect of the DT on the chemical composition was insignificant. The crystal structure was a face-centered cubic (fcc) and the preferred growth orientation was in the [111] direction irrespective of the DT. The crystallization of the samples improved, the size of the crystallites increased and the strength of the [111] growth orientation diminished with the DT. An increment in the DT resulted in a strong enhancement in the particle size and surface roughness. Further surface analysis indicated that the sample surface had a well spread out height distribution at the DT of 40 °C, while the sample surfaces at lower DTs 20 and 30 °C had narrow height distributions. In addition to that, the peaks were found to be predominant on the sample surfaces at lower DTs (20 and 30 °C), whereas the deep valleys were predominant on the sample surface at the DT of 40 °C. Magnetic measurements confirmed the existence of a semi-hard magnetic property in all samples. Compared to other samples produced at lower DTs (20 and 30 °C), the Ni-Fe sample electroplated at the DT of 40 °C possessed the highest coercive force and squareness values. Moreover, the magnetic characteristics of the samples were compatible with their morphological and structural characteristics.

(Received September 30, 2020; Accepted January 11, 2021)

**Keywords:** Ni-Fe/ITO samples, Structural features, Deposition temperature, Particle size, Roughness parameters, Coercive force, Squareness

### 1. Introduction

Ferromagnetic Ni and Ni-Fe samples have been used in a wide range of industrial and technological applications because of their beneficial mechanical, structural and magnetic properties [1–7]. Electrochemical deposition technique has been widely preferred in the manufacturing process of magnetic Ni-Fe samples owing to its well-known economic and technical advantages [7–10]. Furthermore, the chemical composition and physical properties can be tuned by controlling the experimental variables such as deposition potential [11, 12], additive agents [13, 14], solution pH [15, 16, 17], metal ion concentration [11, 16–19], current density [13, 18–21] and DT [17, 21–23]. This opens up a space for producing Ni-Fe samples exhibiting various compositions, morphologies, structural, mechanical and magnetic properties. Apart from the experimental variables mentioned above, the type and features of the substrate used in the manufacturing process affect the properties of the samples grown by electrochemical deposition technique [24–26]. Based on the literature, it is clear that among the substrates, indium tin oxide (ITO)-covered glasses having relatively high transparency and sufficient conductivity are widely utilized in the electrochemical manufacturing process of various types of semiconductor and

---

\* Corresponding author: [usarac@bartin.edu.tr](mailto:usarac@bartin.edu.tr)

magnetic thin films and coatings. In previous investigations of the Ni–Fe samples grown onto ITO–covered glasses, the effects of deposition potential and Fe ion concentration [11], solution pH and NiSO<sub>4</sub>/FeSO<sub>4</sub> molar ratio [16] and deposit thickness [27] were examined. To our best knowledge, to date, no studies investigating the impact of the DT on the properties of the ferromagnetic Ni–Fe/ITO samples have yet been performed. The purpose of this investigation, therefore, is to examine the influence of the DT on the properties of the Ni–Fe/ITO thin film samples such as Fe concentration, particle size, roughness parameters, coercive force, squareness, crystallite size, lattice parameter, texture strength and crystallization. The results obtained under the study revealed the role of the DT on the Ni–Fe thin film samples electrochemically coated onto glasses covered with ITO for the first time.

## 2. Experimental

In this research, thin film samples of Ni–Fe were electrochemically fabricated at various DTs in the range of 20 and 50 °C by means of the potentiostat/galvanostat (VersaSTAT 3) in a three–electrode cell composed of counter, reference and working electrodes at a constant current density of  $-20 \text{ mA/cm}^2$ . A platinum sheet with an area of  $1.5 \text{ cm}^2$ , a saturated calomel electrode (SCE) and a conductive ITO–coated glass were utilized as a counter electrode, a reference electrode and a working electrode, respectively. Freshly prepared solutions containing sulfate salts of 0.070 M Ni and 0.0030 M Fe were used in production processes of the samples. 0.1 M boric acid was also added to the sulfate–based solutions to ensure the stability of pH during electrochemical deposition of the samples. The solutions had a pH value of  $5 \pm 0.1$ . The cleaning process of the ITO–coated glasses having a sheet–resistance of 8–12  $\Omega/\text{sq}$  and a working area of  $1 \text{ cm}^2$  was first performed by an acetone solution for 10 minutes and immediately an ethanol solution for 10 minutes. After this process, the surfaces of the ITO–coated glasses were rinsed by an ultrasonic bath for 15 minutes. The samples had a thickness of about 450 nm. The growth process of the samples was also followed via galvanostatic potential–time transients recorded during electrochemical deposition process.

X–ray diffractometer (XRD, Rigaku Smart LabTM) was used to examine the influence of the DT on the crystal structure, texture formation, crystallite size and texture evolution. During XRD measurements, the scan was done in the range of 40°–55° with 0.01° steps using a Cu–K $\alpha$  radiation with  $\lambda = 0.15406 \text{ nm}$ . The coercive force and squareness values of the samples were determined using a vibrating sample magnetometer (VSM, JDAW–2000D model). During magnetic measurements, the magnetic field was applied along the in–plane direction at ambient temperature and pressure. To investigate the influences of the DT on the morphology and concentration of the samples a scanning electron microscopy (SEM, Tescan MAIA3 XMU) and an energy dispersive X–ray spectroscopy (EDX) were used, respectively. An atomic force microscopy (AFM, MultiMode V SPM of Veeco) was also used to explore the impact of the DT on the particle size and surface roughness parameters. To determine the surface roughness parameters such as surface kurtosis, surface skewness, root–mean–square (rms) and average surface roughness AFM micrographs were analyzed in detail by means of the WSxM software package (Version 5.0) [28].

## 3. Results and discussion

The recorded galvanostatic potential–time transients for various DTs are illustrated in Fig. 1. It was observed that all cathode potentials were stable during deposition process, reflecting the uniform electrochemical deposition. However, the highest value of the cathode potential was observed at the lowest DT of 20 °C, while the cathode potential reached the lowest value at the highest DT of 50 °C relative to other DTs. Similar results were also reported in electrochemically fabricated Ni Here, it is worth noting that the electrochemical fabrication of a proper Ni–Fe/ITO sample at the DT of 50 °C is not possible due to its brittle properties. A possible reason for that can be an inappropriate cathode potential. In a previous study [11], the binary Ni–Fe/ITO samples

could be successfully fabricated at the cathode potentials  $\geq -1.2$  V versus SCE. This can be also used to explain the brittle feature of the sample electrochemically deposited at the DT of 50 °C since the cathode potential for this sample was lower than  $-1.2$  V versus SCE. On the other hand, the impact of the DT on the Fe concentration was evaluated by the EDX analysis. The results indicated a very slight increase in the Fe concentration of the samples from 4.8 to 6.0 at.% when the DT was raised from 20 to 40 °C, indicating an insignificant effect of the DT on the Fe concentration of the Ni–Fe/ITO thin film samples (Table 1). This result is consistent with the result of the published study performed by Kim et al [17]. In that study, it was shown that there was no a significant change in the Fe concentration of the Ni–Fe deposits when the DT was varied, under 45 °C. However, different results were also documented in the literature regarding the effect of the DT on the Fe concentration. For instance, Lee et al. showed that the DT played a significant role on the Fe concentration of the Ni–Fe deposits [22]. Furthermore, the Fe concentration in the deposits decreased when the DT was raised. However, the study carried out by Yin et al. revealed that raising temperature led to an enhancement in the Fe concentration in the samples [23].

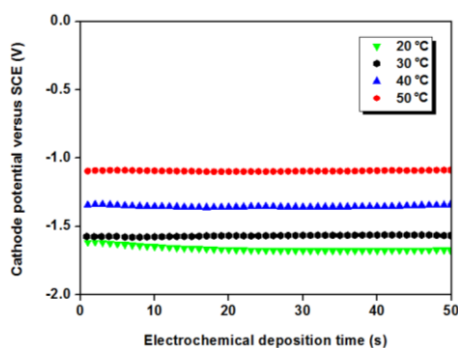


Fig. 1. Galvanostatic potential–time transients for various DTs recorded during electrochemical deposition.

In the present work, Ni–Fe/ITO thin film samples were reproduced from an electrolyte with higher Fe ions (0.0060 M) under the same conditions to verify the effect of DT on the chemical composition of the samples. As reported in previous works [11, 16], the films electroplated from the electrolyte with the higher Fe ions (0.0060 M) contained higher Fe concentration than the films deposited from the electrolyte with lower Fe ions (0.0030 M) at all DTs. However, there was a very slight increment in the Fe concentration of the samples from 9.0 to 9.8 at.% when the DT was increased from 20 to 40 °C, confirming an insignificant effect of the DT on the Fe concentration of the Ni–Fe/ITO thin film samples for the conditions applied in this work.

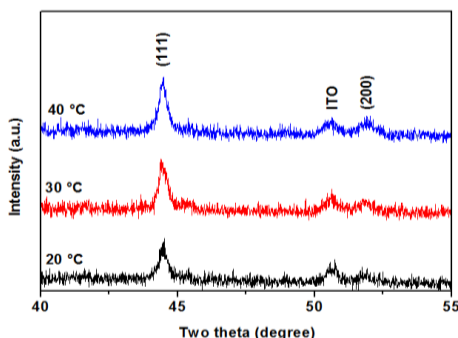


Fig. 2. XRD patterns of the electrochemically deposited thin films.

The XRD patterns are demonstrated in Fig. 2. All of the produced samples exhibited the (111) and (200) diffraction peaks of the fcc crystal structure. Raising DT induced an enhancement in the peak intensities of both (111) and (200) crystal planes, revealing that the crystallization of the samples improved with the DT. Similar effect of DT on the crystallization was also reported in former studies for both Ni–Fe [21] and Ni–Co [29] deposits. On the other hand, as distinctly noticed from the XRD patterns shown in Fig. 2, there was a decrement in the intensity of the ITO diffraction peak with increasing DT. This indicated an increase in the current efficiency when the DT was increased, resulting in an enhancement in the thickness of the samples. The study showed that the intensity of the ITO diffraction peaks decreased as the thickness of the FeNi/ITO thin films increased [27]. An increase in the Ni–Cu/ITO film thickness was also reported as the DT was raised [30], supporting our findings. To estimate the crystallite size, the XRD diffraction patterns were fitted by Lorentzian curves as demonstrated in Fig. 3 for the sample grown at 40 °C. The size of the crystallites was estimated using Scherrer equation [31]:

$$D = [0.9\lambda / \text{FWHM}\cos\theta] \times [180^\circ / \pi]$$

where FWHM is the full width at half maximum of the (111) diffraction peak,  $\lambda$  is the wavelength of Cu–K $\alpha$  radiation,  $\theta$  is the diffraction angle and  $D$  is the size of the crystallites. The analysis showed that the size of the crystallites increased from 20.5 to 23.9 nm as the DT was enhanced from 20 to 40 °C (Table 1). The increase in the size of the crystallites can be due to a decrease in the cathode potential with raising DT as seen from Fig. 1. It is well known that a decrement in the cathode potential results a decrease in the nucleation rate due to an enhancement in the energy of nucleus formation [29, 32–38]. Therefore, an increase in the DT leads to an increment in the size of the crystallites, which is consistent with the results of former works documented in the literature for different material systems [29, 32, 36, 38–41]. From the structural analysis, it was also observed that as the DT was increased from 20 to 40 °C, the (111) diffraction peak position shifted slightly to a lower angle. As demonstrated in Table 1, this led to a small increase in the lattice constant of the samples, which was consistent with a very slight increase in the Fe concentration of the samples. This is because the lattice constant of fcc Fe (111) is larger than that of fcc Ni (111) [11, 42–46].

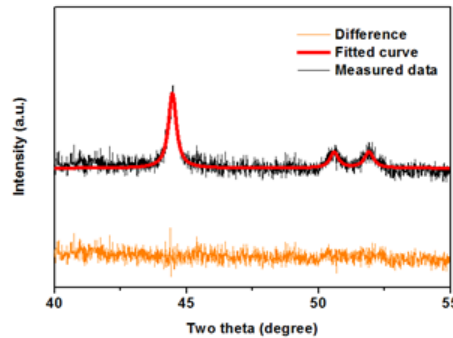


Fig. 3. Lorentz fitting the sample grown at the DT of 40 °C.

We also examined the role of the DT on the crystallographic texture formation and texture strength. To reveal the texture formation and its evolution depending on the DT, the intensity ratio,  $I_{(111)}/I_{(200)}$ , was obtained for each deposit. The obtained values of the  $I_{(111)}/I_{(200)}$  are shown in Fig. 4 against the DT. The  $I_{(111)}/I_{(200)}$  value for a sample comprising the crystallites with randomly oriented is also depicted in Fig. 4 [47]. The  $I_{(111)}/I_{(200)}$  values of the studied Ni–Fe samples were always higher than that of the sample with randomly oriented crystallites. This meant that all resultant samples had a [111] preferred crystallographic orientation. However, an increment in the DT induced a strong decrease in the  $I_{(111)}/I_{(200)}$  ratio, indicating a noticeable reduction in the strength of the [111] texture. The change of the texture strength is related to the adsorption of hydrogen and hydroxide species on a preferential crystallographic plane [30, 41, 48–51], which gives rise to the formation of growth rate anisotropy [41, 48]. Furthermore, a decrement in the

strength of the [111] texture resulted in an increment in the size of the crystallites, which was consistent with the results of the recently published work [41].

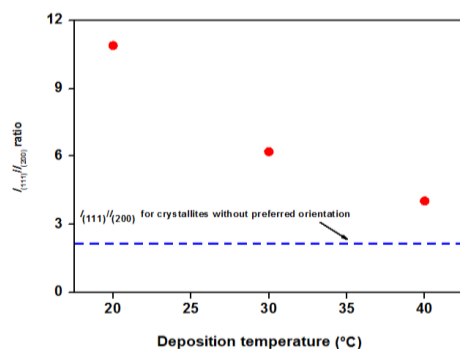


Fig. 4.  $I_{(111)}/I_{(200)}$  values against the DT.

The morphologies of the samples were explored using both SEM and AFM characterization techniques depending on the DT. The SEM (Fig. 5) and the AFM images (Fig. 6) indicated that the sample surfaces were uniformly covered with various sizes of nodular particles irrespective of the DT. However, at the DT of 20 °C, the sample exhibited the smallest nodular particles varying between 70 and 120 nm. The width of the nodular particles continued to increase as the DT was increased from 20 to 30 °C. The width of the nodular particles at the DT of 30 °C ranged from 100 to 200 nm. Further increase in the DT from 30 to 40 °C caused a further reduction in the nucleation rate and therefore led to a further enhancement in the width of the nodular particles. The width of nodular particles of the sample grown at the DT of 40 °C was in the range of 180 to 300 nm. In a former study [21], the influence of the DT on the surface morphology of the Ni–Fe samples was also explored. Contrary to our results, it was found that the grain size reduced when the DT was enhanced from 50 to 70 °C. This may arise from different parameters applied in the experiments such as electrolyte concentration, current density and substrate type, as well as the range of DT.

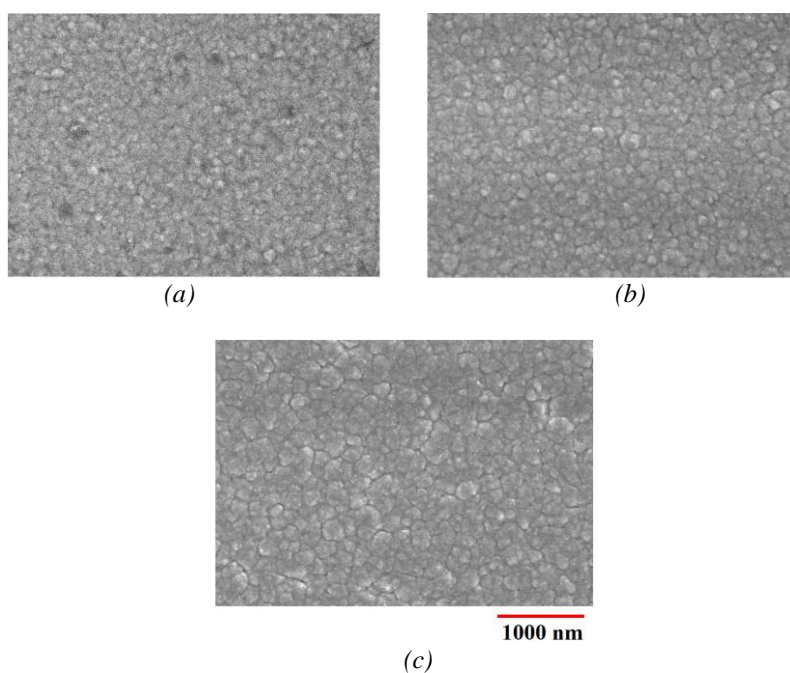


Fig. 5. SEM micrographs of the electrochemically coated Ni–Fe thin film samples for different DTs a) 20 °C, b) 30 °C and c) 40 °C, respectively.

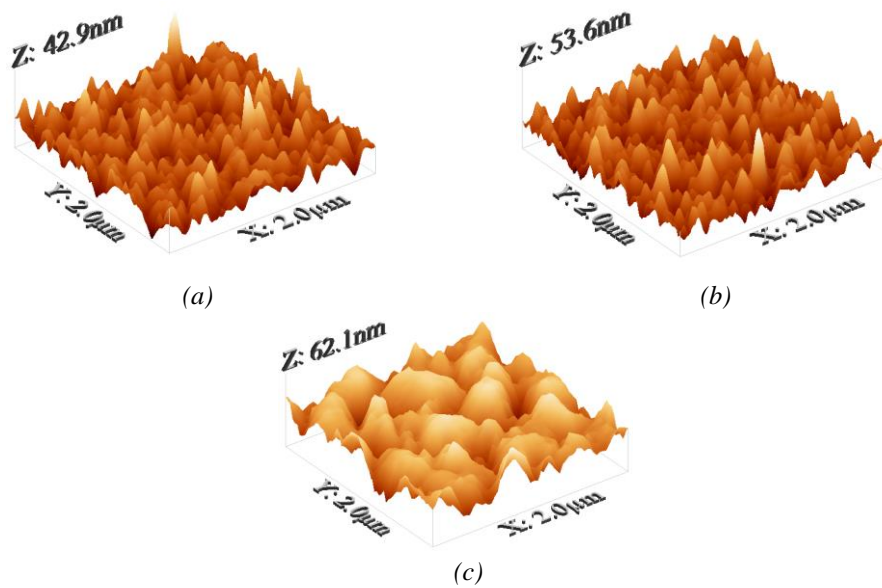


Fig. 6. AFM micrographs of the electrochemically produced Ni–Fe thin film samples for various DTs a) 20 °C, b) 30 °C and c) 40 °C, respectively.

To reveal the impact of the DT on the roughness parameters such as surface kurtosis, surface skewness, rms surface roughness and average surface roughness further detailed surface analysis was carried out. The evolution of the surface roughness is depicted in Fig. 7 with respect to the DT. A significant increase in the average and rms surface roughness of the samples was observed with raising DT, which can be attributed to the increase in the size of the nodular particles. On the other hand, the height distribution histograms of the samples are shown in Fig. 8. The determined surface skewness and kurtosis values, which are utilized for the characterization of the height asymmetry [52–56], are demonstrated in Fig. 9a and b, respectively. The skewness and kurtosis values for a Gaussian distribution are also depicted in the figures [54–57]. The samples deposited at the DTs of 20 and 30 °C had positive skewness values while the sample grown at the DT of 40 °C had a negative skewness value (Fig. 9a), indicating that the surface height distributions do not follow a Gaussian distribution [58]. This indicated that the peaks were predominant on the sample surfaces at 20 and 30 °C, while the deep valleys were predominant on the sample surface at 40 °C [54–59]. On the other hand, the samples fabricated at the DTs of 20 and 30 °C exhibited a surface kurtosis value higher than 3, whereas the sample deposited at the DT of 40 °C possessed a surface kurtosis value lower than 3 (Fig. 9b). This meant that the sample surfaces have a narrow height distribution at 20 and 30 °C, whereas the surface of the sample showed a well spread out height distribution at 40 °C [55, 60]. Thus, it is concluded that the DT plays a significant role on the height asymmetry of the sample surfaces.

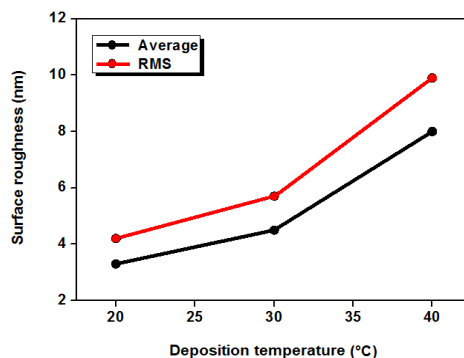


Fig. 7. Surface roughness of the samples against the DT.

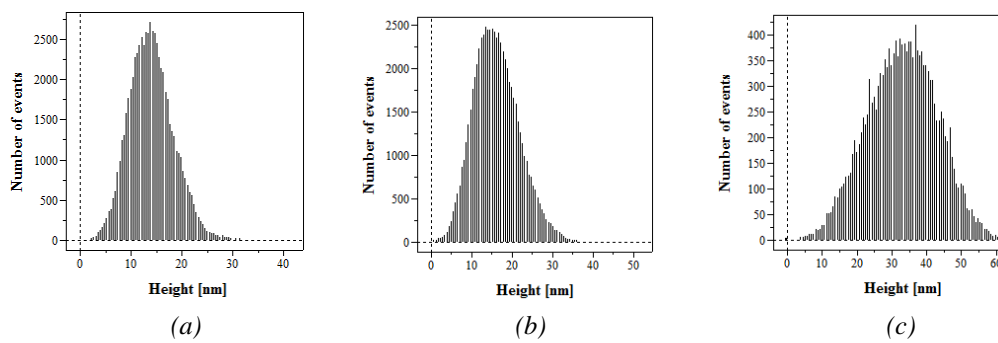


Fig. 8. Height distribution histograms of the electrochemically coated Ni–Fe thin film samples for various DTs a) 20 °C, b) 30 °C and c) 40 °C, respectively.

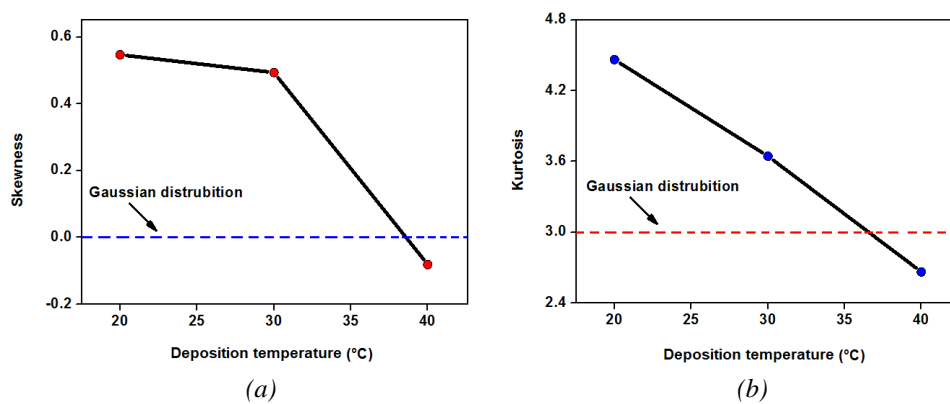


Fig. 9. Skewness and kurtosis values as a function of the DT.

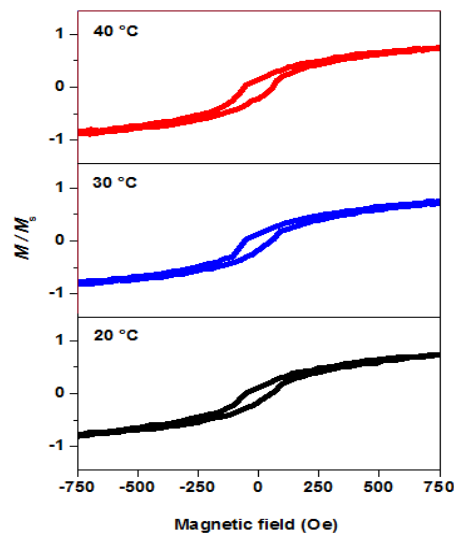


Fig. 10. Normalized in–plane magnetic hysteresis loops of the electrochemically coated Ni–Fe thin film samples for various DTs.

The in–plane magnetic hysteresis loops are shown in Fig. 10 and the obtained squareness ( $M_r/M_s$ , where  $M_r$  is the remanent magnetization and  $M_s$  is the saturation magnetization) and coercive force values are listed in Table 1. The results revealed that the squareness value of the samples increased slightly with the DT. The squareness values of the samples were found to be

0.0880, 0.0935 and 0.1050 for the samples deposited at the DTs of 20, 30 and 40 °C, respectively. In addition, all resultant samples were observed to have a semi-hard magnetic feature, whereas raising DT from 20 to 40 °C induced an increment in the coercive force ( $H_c$ ) from 53 to 59 Oe. It should also be noted that the variations observed in the particle and crystallite sizes and surface roughness values are compatible with the variation detected in the coercive force. This indicated that larger particle and crystallite sizes and higher surface roughness values contributed to the observed increase in the coercive force. Similar findings were also reported in electrochemically fabricated Fe-Co-Ni/ITO thin films [61].

*Table 1. The compositional, structural and magnetic properties with respect to the DT.*

DT (°C)	Composition (at.%)		Crystallite size (nm)	Lattice parameter (nm)	$H_c$ (Oe)	$M_r/M_s$
	Fe	Ni				
20	4.8	94.9	$20.5 \pm 0.9$	$0.352735 \pm 48 \times 10^{-6}$	53	0.0880
30	5.5	94.2	$21.2 \pm 0.7$	$0.352795 \pm 35 \times 10^{-6}$	55	0.0935
40	6.0	93.7	$23.9 \pm 0.7$	$0.352812 \pm 28 \times 10^{-6}$	59	0.1050

#### 4. Conclusions

This paper reported the role of the DT on the Fe concentration, particle size, roughness parameters, coercive force, squareness and structural features of the ferromagnetic Ni-Fe samples electrochemically deposited onto glasses covered with ITO. Diffraction patterns confirmed the formation of the fcc crystal structure with the preferential orientation along the [111] direction in all samples. Increasing DT induced an improvement in the crystallization. The crystallite size of the (111) plane increased from 20.5 to 23.9 nm and the strength of the [111] texture decreased as the DT was increased from 20 to 40 °C. The effect of the DT on the Fe concentration of the Ni-Fe/ITO thin film samples was found to be insignificant. There was a very slight enhancement in the Fe concentration from 4.8 to 6.0 at.% with rising DT; this was also consistent with the slight increase observed in the lattice constant from 0.352735 to 0.352812 nm. Morphological analysis performed using a SEM and an AFM showed that the sample surfaces were uniformly coated with nodular particles of different sizes. However, the nodular particle size continued to increase as the DT was increased.

The surface roughness of the samples also increased with the DT. Further detailed studies carried out on the AFM micrographs indicated that the sample surface had a well spread out height distribution and the deep valleys were predominant at the DT of 40 °C. However, the sample surfaces possessed narrow height distributions and the peaks were predominant at lower DTs of 20 and 30 °C. Magnetic measurements confirmed that all samples exhibited a semi-hard magnetic feature. Furthermore, raising DT from 20 to 40 °C resulted in an increase in the coercive force and squareness from 53 to 59 Oe and from 0.0880 to 0.1050, respectively. The analysis also revealed that larger particle and crystallite sizes and higher surface roughness values induced a higher coercive force in the samples.

#### Acknowledgements

This work was financially supported by the Scientific Research Projects Commission of Bartın University under the project number 2018-FEN-A-021. The authors wish to thank Çağdaş Denizli for taking AFM micrographs.

## References

- [1] V. Torabinejad, M. Aliofkhaezaei, S. Assareh, M. H. Allahyarzadeh, A. S. Rouhaghdam, *J. Alloys Compd.* **691**, 841 (2017).
- [2] S. Arabi, G. Avramovic–Cingara, G. Palumbo, U. Erb, M. Niewczas, *Mater. Sci. Forum* **706-709**, 1642 (2012).
- [3] G. Maizza, H. Eom, M. Lee, T. H. Yim, E. Nakagawa, R. Pero, T. Ohmura, *J. Mater. Sci.* **54**, 13378 (2019).
- [4] H. Gong, M. Rao, D. E. Laughlin, D. N. Lambeth, *J. Appl. Phys.* **85**, 5750 (1999).
- [5] I. Matsui, T. Kawakatsu, Y. Takigawa, T. Uesugi, K. Higashi, *Mater. Lett.* **116**, 71 (2014).
- [6] M. Nawaz Rizwan, M. A. Kalyar, C. Bell, M. Anwar-Ul-Haq, A. R. Makhdoom, *Dig. J. Nanomater. Biostructures*, **15**, 1141 (2020)
- [7] T. Shimokawa, T. Yanai, K. Takahashi, M. Nakano, K. Suzuki, H. Fukunaga, *IEEE Trans. Magn.* **48**, 2907 (2012).
- [8] B. Subramanian, K. Govindan, V. Swaminathan, M. Jayachandran, *Trans. Inst. Metal Finish.* **87**, 325 (2009).
- [9] M. Ghorbani, A. G. Dolati, A. Afshar, *Russ. J. Electrochem.* **38**, 1173 (2002).
- [10] S. Fazli, M. E. Bahrololoom, *Metall. Mater. Trans. A* **47A**, 4316 (2016).
- [11] U. Sarac, M. Kaya, M. C. Baykul, *Turk. J. Phys.* **41**, 536 (2017).
- [12] A. A. Frey, N. R. Wozniak, T. B. Nagi, M. P. Keller, J. M. Lunderberg, G. F. Peaslee, P. A. DeYoung, J. R. Hampton, *Int. J. Electrochem.* **2011**, 604395 (2011).
- [13] Y. Kashiwa, N. Nagano, T. Takasu, S. Kobayashi, K. Fukuda, H. Nakano, *ISIJ Int.* **59**, 514 (2019).
- [14] S.-H. Kim, H.-J. Sohn, Y.-C. Joo, Y.-W. Kim, T.-H. Yim, H.-Y. Lee, T. Kang, *Surf. Coat. Technol.* **199**, 43 (2005).
- [15] P. Fricoteaux, C. Rousse, *J. Electroanal. Chem.* **612**, 9 (2008).
- [16] X. Su, C. Qiang, *Bull. Mater. Sci.* **35**, 183 (212).
- [17] J.-H. Kim, T. Yim, J.-H. Lee, *Curr. Appl. Phys.* **13**, S108 (2013).
- [18] M. Moniruzzaman, K. M. Shorowordi, A. Azam, M. F. N. Taufique, *J. Mech. Eng.* **44**, 51 (2014).
- [19] Y.-Hua Zhang, G.-Fu Ding, Y.-Li Cai, H. Wang, B. Cai, *Mater. Charact.* **57**, 121 (2006).
- [20] T. Yanai, T. Shimokawa, Y. Watanabe, T. Ohgai, M. Nakano, K. Suzuki, H. Fukunaga, *J. Appl. Phys.* **115**, 17A325 (2014).
- [21] Y. Cao, G. Y. Wei, H. L. Ge, X. F. Meng, *Surf. Eng.* **30**, 97 (2014).
- [22] T.-R. Lee, L. Chang, C.-H. Chen, *Surf. Coat. Technol.* **207**, 523 (2012).
- [23] K.-M. Yin, S.-L. Jan, C.-C. Lee, *Surf. Coat. Technol.* **88**, 219 (1997).
- [24] J. B. Yi, X. P. Li, J. Ding, H. L. Seet, *J. Alloys Compd.* **428**, 230 (2007).
- [25] E. I. Manimaran, K. Antonyraj, E. R. Navaneetha, V. S. Kumar, P. Rajesh, *J. Mater. Sci. Mater. Electron.* **29**, 3715 (2018).
- [26] L. Nzoghe–Mendomea, A. Aloufy, J. Ebothé, M. ElMessiry, D. Hui, *J. Cryst. Growth* **311**, 1206 (2009).
- [27] D. Cao, Z. Wang, E. Feng, J. Wei, J. Wang, Q. Liu, *J. Alloys Compd.* **581**, 66 (2013).
- [28] I. Horcas, R. Fernández, J. M. G.-Rodríguez, J. Colchero, J. G. Herrero, A. M. Baro, *Rev. Sci. Instrum.* **78**, 013705 (2007).
- [29] U. Sarac, M. Kaya, M. C. Baykul, *Applied Physics A* **126**, 1 (2020).
- [30] U. Sarac, M. C. Baykul, *J. Alloys Compd.* **552**, 195 (2013).
- [31] J. Wang, W. Lei, Y. Deng, Z. Xue, H. Qian, W. Liu, X. Li, *Surf. Coat. Technol.* **358**, 765 (2019).
- [32] U. Sarac, M. C. Baykul, *J. Mater. Sci. Mater. Electron.* **24**, 952 (2013).
- [33] S. Armyanov, S. Vitkova, O. Blajiev, *J. Appl. Electrochem.* **27**, 185 (1997).
- [34] A. M. Rashidi, A. Amadeh, *Surf. Coat. Technol.* **204**, 353 (2009).
- [35] A. M. Rashidi, A. Amadeh, *J. Mater. Sci. Technol.* **26**, 82 (2010).
- [36] V. C. Nguyen, C. Y. Lee, L. Chang, F. J. Chen, C. S. Lin, *J. Electrochem. Soc.* **159**, D393 (2012).
- [37] E. Budevski, G. Staikov, W. J. Lorenz, *Electrochim. Acta* **45**, 2559 (2000).

- [38] H. Natter, R. Hempelmann, *Electrochim. Acta* **49**, 51 (2003).
- [39] U. Sarac, M. C. Baykul, *Dig. J. Nanomater. Biostruct.* **9**, 1179 (2014).
- [40] W. H. Li, X. Y. Zhou, Z. Xu, M. J. Yan, *Surf. Eng.* **25**, 353 (2009).
- [41] L. Feng, Y. Yue-Ren, Y. H. Zhang, S. Wang, L. Li, *Metals* **9**, 1 (2019).
- [42] X. Liu, G. Zangari, M. Shamsuzzoha, *J. Electrochem. Soc.* **150**, C159 (2003).
- [43] U. Sarac, M. C. Baykul, *J. Mater. Sci. Mater. Electron.* **25**, 2554 (2014).
- [44] Y. A. Zaharov, V. M. Pugachev, V. I. Ovcharenko, K. A. Dativ, A. N. Popova, A.S. Bogomyakov, *Phys. Status Solidi B* **255**, 1700175 (2018).
- [45] H. Li, F. Ebrahimi, *Mater. Sci. Eng. A* **347**, 93 (2003).
- [46] S. D. Leith, S. Ramli, D. T. Schwartz, *J. Electrochem. Soc.* **146**, 1431 (1999).
- [47] B. D. Cullity, *Elements of X-Ray Diffraction*, Addison-Wesley, London (1978).
- [48] C. Savall, A. Godon, J. Creus, X. Feaugas, *Surf. Coat. Technol.* **206**, 4394 (2012).
- [49] M. Hacıismailoglu, M. Alper, *Surf. Coat. Technol.* **206**, 1430 (2011).
- [50] M. Boubatra, A. Azizi, G. Schmerber, A. Dinia, *Ionics* **18**, 425 (2012).
- [51] S. Tebbakh, Y. Messaoudi, A. Azizi, N. Fenineche, G. Schmerber, A. Dinia, *Trans. IMF* **93**, 196 (2015).
- [52] G. Yildirim, S. Bal, M. Gulen, A. Varilci, E. Budak, M. Akdogan, *Cryst. Res. Technol.* **47**, 195 (2012).
- [53] G. P. Daniel, V. B. Justinvictor, P. B. Nair, K. Joy, P. Koshy, P. V. Thomas, *Phys. B* **405**, 1782 (2010).
- [54] M. Nenadović, S. Štrbac, Z. Rakočević, *Appl. Surf. Sci.* **256**, 1652 (2010).
- [55] U. Sarac, M. C. Baykul, *J. Mater. Sci. Mater. Electron.* **25**, 39 (2014).
- [56] M. Sedlaček, B. Podgornik, J. Vižintin, *Tribol. Int.* **48**, 102 (2012).
- [57] B. Ma, A. K. Tieu, C. Lu, Z. Jiang, *J. Mater. Process. Tech.* **125-126**, 657 (2002).
- [58] S. S. Lekshmy, G. P. Daniel, K. Joy, *Appl. Surf. Sci.* **274**, 95 (2013).
- [59] S. Rajendran, K. K. Karuppanan, R. Pezhinkattil, *Micron* **43**, 1299 (2012).
- [60] V. K. Truong, R. Lapovok, Y. S. Estrin, S. Rundell, J. Y. Wang, C. J. Fluke, R. J. Crawford, E. P. Ivanova, *Biomaterials* **31**, 3674 (2010).
- [61] U. Sarac, M. Kaya, M. C. Baykul, *J. Supercond. Nov. Magn.* **32**, 917 (2019).